CHEMISTRY
A EUROPEAN JOURNAL

DOI: 10.1002/chem.200601784

Optimal Attachment Position and Linker Length Promote Native-like Character of Cavitand-Based Template-Assembled Synthetic Proteins (TASPs)

Emily S. Seo, Walter R. P. Scott, Suzana K. Straus, and John C. Sherman*[a]

Abstract: We have designed, synthesised and characterised a series of template-assembled de novo four-helix bundles, each differing in the linker length between the template and the peptides. The helix is based on an earlier peptide sequence: EELLKKLEELLKKLG (first-generation sequence), which was designed to link the hydrophilic/hydrophobic interface of the helices. Increasing or decreasing the linker length by one glycine residue had a significant effect on the structure and properties of the template-assembled synthetic proteins (TASPs). Here, the effect of the linker length is further probed by linking the peptides closer to the hydrophobic face by using the second-generation sequence, AEELLKKLEELLKKG, in an effort to improve the packing between the helices and to better understand the helical bundles. The peptides were synthesised with 0–4 Gly linker residues and linked onto a cavitand template. The proteins were found to be α-helical, stable to guanidine hydrochloride (GuHCl) and to unfold cooperatively. However, their stabilities toward GuHCl, propensity to self-aggregate and structural specificity differed. The two-glycine variant of the second-generation series demonstrated the highest stability and most native-like character of all the mononeric TASPs in both the first- and second-generation series. The structural specificity of this two glycine variant is comparable to that of other known native-like de novo proteins. Molecular dynamics simulations showed that the two-glycine variant contains helices that are tilted with respect to the cavitand template and may account for its unique properties.

Keywords: cavitands · helical structures · molecular dynamics · protein design · synthetic proteins · template synthesis

Introduction

The protein-folding problem, which is the prediction of tertiary structure from primary amino acid sequence, has been an ongoing challenge to solve. An approach to studying protein folding is to employ de novo design, which involves the engineering of a protein from scratch.[1,2] Although smaller than their natural counterparts, de novo proteins contain much of the same elements involved in folding, and thus can be used as simpler models to study protein structure. A particularly useful type of de novo design is template-assembled synthetic proteins (TASPs).[2] The template can simplify a structure by reducing the number of loops and turns, and it can also aid in increasing the helicity and stability of the overall protein with respect to non-linked peptides.[2c,3] A challenge associated with examination of protein structures is to distinguish the features responsible for dictating a well-packed, native-like protein as opposed to a molten-globule structure, which lacks the specific tertiary interactions between the side chains. Four-helix bundles that contain the same non-polar residues in the hydrophobic core tend to display molten-globule characteristics;[4] increasing the diversity of the hydrophobic core of the bundle has been found to increase the native-like properties.[5] Although replacing the non-polar residues with polar residues can destabilise the overall structure, the charged residues can be essential to the formation of native protein structures.[6] On the other hand, binary-patterned libraries, which constrain the positions of the polar and non-polar residues but vary

[a] Dr. E. S. Seo, Dr. W. R. P. Scott, Assist. Prof. S. K. Straus, Prof. J. C. Sherman
Department of Chemistry, University of British Columbia
2036 Main Mall, Vancouver, BC, V6T 1Z1 (Canada)
Fax: (+1) 604)822-2847
E-mail: sherman@chem.ubc.ca

Supporting information for this article is available on the WWW under http://www.chemistry.org or from the author. It includes the sedimentation equilibria data, including plots of absorbance versus radius and the residuals for each plot. The 2D ^{1}H NMR spectra used to assign the amide-proton resonances and the tables of the assigned signals are included. The stack plots of the N-H/D exchange spectra are also available. For the MD simulation results, the Ramachandran plots are included.

the identity of the side chains, have also produced well-ordered structures.[7,8] Furthermore, the length of the loops connecting helices in coiled coil[9] and bundle[10] structures, or the linker length between the template and the peptides (in the case of TASPs)[11] were found to have profound effects on the stability and properties of the proteins. However, these findings have not been studied in detail. Previously, our group used a cavitand template[12] to study the effect of the linker length. This earlier study consisted of a series of four-helix bundles called caviteins (**cavi**tand template + pro**teins**)[13] that differed in the number of glycine linkers between the template and the peptides (see Scheme 1). The

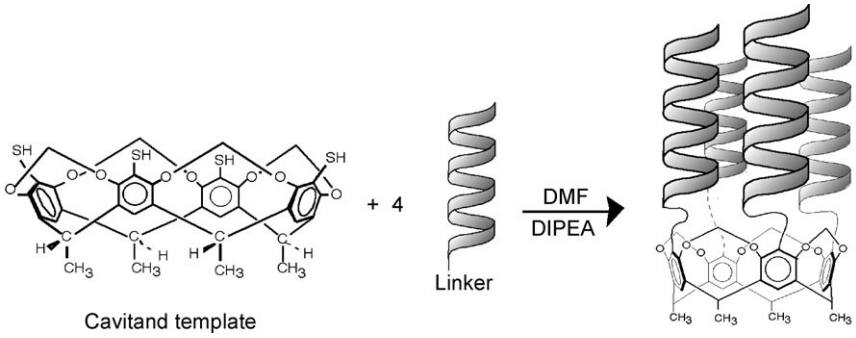

Scheme 1. Cavitein synthesis.

first-generation peptides with the sequence **S1** (i.e., EELLKKLEELLKKG, which was designed to link the hydrophilic/hydrophobic interface) were synthesised with 0–3 Gly units and linked onto the cavitand template.[14] This study showed that the linker length had a significant effect on the tertiary and quaternary structure of the proteins.[14] The cavitand template was effective in inducing native-like properties in the protein bundles, even with a peptide sequence containing an all Leu core.[14] From the first-generation series, 2 to 3 Gly residues were required in the linker region to generate a well-defined cavitein. Here, the effect of the linker length is further investigated by examining a different linkage point of the peptides to the cavitand. This second-generation peptide sequence, **S2** (i.e., AEELLKKLEELLKG), was designed so that the attachment point begins closer to the hydrophobic face of the helix. The goals are to study the factors that affect the native-like character of these de novo proteins and to determine if initiating the linkage closer to the hydrophobic face would improve the packing, and consequently result in proteins with improved native-like character. In addition, by examining and comparing the first- and second-generation series, we attempt to better understand the four-helix bundle systems.

Results and Discussion

Design: The second-generation peptide sequence was based on the first-generation sequence with the addition of an alanine residue at the N terminus to give sequence **S2**, AEELLKKLEELLKKG. This sequence was intended to place the linker at the hydrophobic region of the helix, whereas the first-generation presumably linked at the interface of the hydrophobic and hydrophilic faces as illustrated in Figure 1. The peptide sequence for both generations was designed based on the minimalist approach,[15] in which the only non-polar residues are Leu (excluding Ala) and the only polar residues are Glu and Lys; 0–4 Gly linkers are also added onto the N terminus and a Gly residue is used to cap the C terminus.[16] The negatively charged Glu residues and positively charged Lys residues are placed three to four residues apart for optimal intrahelical salt-bridge formation. The C terminus was amidated in order to minimise charge–charge repulsion between the helices and to reduce the macrodipole effect.[13]

The template used by our group is a cavitand—a rigid macrocycle with an enforced cavity.[17] A cavitand can be synthesised with a variety of functional groups at the "rim" and "foot" positions.[18] Specifically, the arylthiol-rimmed cavitand template with methyl "feet" was employed here.[13] The rim positions are spaced approximately 7 Å apart, and are within the range of natural interhelical distances, which are between 7 to 14 Å.[19] Furthermore, a cavitand template can regulate the number of helices in a bundle as determined by the number of functional groups, and can control the orientation of the helices in a parallel arrangement.

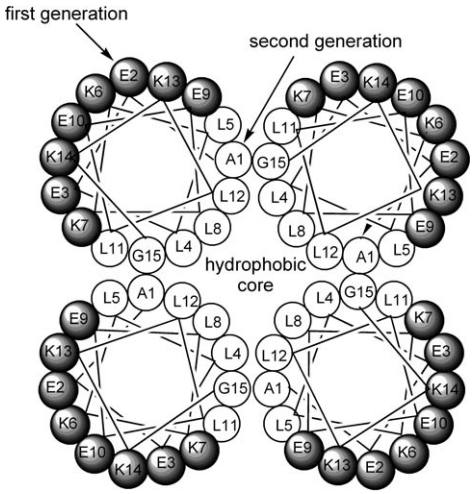

Figure 1. Helix-wheel diagram showing putative first- and second-generation linkage points.

Synthesis: The peptides were generated by using standard solid-phase peptide synthesis. For peptides **1**–**5**, the N termini of the corresponding peptide resins underwent reaction with chloroacetyl chloride, while the reactive side groups and C termini remained protected. For the reference peptide **6**, the free N terminus of the peptide resin underwent reaction with acetic anhydride. Peptide **6** remains unlinked to the cavitand. The peptide resins were treated with 95% trifluoroacetic acid (TFA) in order to cleave the resin from the peptides and to remove the protecting groups from the side chains. Table 1 lists the peptides employed in this study.

Table 1. List of peptides used in the synthesis of the caviteins ([peptide] refers to the sequence: AEELLKKLEELLKKG).

Peptide	Sequence
1	$ClCH_2CO$-NH-[Gly][peptide]-$CONH_2$
2	$ClCH_2CO$-NH-[GlyGly][peptide]-$CONH_2$
3	$ClCH_2CO$-NH-[GlyGlyGly][peptide]-$CONH_2$
4	$ClCH_2CO$-NH-[GlyGlyGlyGly][peptide]-$CONH_2$
5	$ClCH_2CO$-NH-[peptide]-$CONH_2$
6	CH_3CO-NH-[peptide]-$CONH_2$

Each activated peptide was reacted with the cavitand template[17] in the presence of dimethylformamide (DMF) and *N*,*N*′-diisopropylethylamine (DIPEA) to afford the corresponding caviteins: 1GS2, 2GS2, 3GS2 and 4GS2 (see Scheme 2). Peptide **5**, with no Gly units at the N terminus, linked onto the cavitand to form the four-helix bundle cavitein; however, the cavitein could not be obtained in pure form and thus was not used in this study.

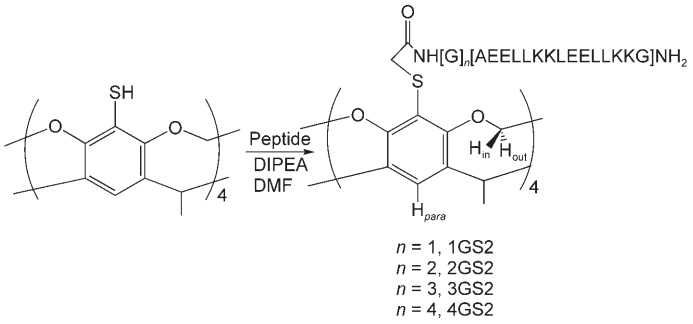

Scheme 2. Synthesis of the second-generation caviteins.

Characterisation: The structure and properties of the caviteins in the second-generation series were analysed by using circular dichroism (CD) spectroscopy, chemical denaturation data, sedimentation equilibria studies, 1D and 2D ^{1}H NMR spectroscopy, N-H/D exchange experiments, hydrophobic-dye binding studies together with fluorescence and molecular dynamics simulations.

Far-UV/CD spectra: All the caviteins possess CD spectra characteristic of α-helices, which include minima at 222 and 208 nm and a maximum at 195 nm (see Figure 2). The α-helical content was not calculated for the caviteins, as aromatic

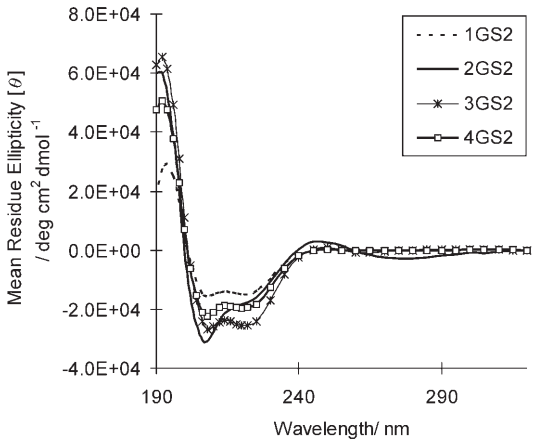

Figure 2. CD spectra of 40 μM cavitein samples in 50 mM phosphate buffer, pH 7.0 at 25 °C.

chromophores (in this case, the cavitand template) are known to affect the mean residue ellipticity at 222 nm.[20] The CD spectra were run at high (40 μM) and low (4 μM) sample concentrations for each cavitein. The caviteins demonstrated concentration independent curves (suggesting single species—vide infra), and therefore only the high-concentration data are shown.

Near-UV/CD spectra: The far-UV/CD spectra give information on the secondary structure of the proteins. The near-UV region of the CD spectra, however, can yield information about the tertiary structure of the protein if a chromophore is present—again, in this case the cavitand template.[21] An aromatic absorption in the near-UV region can be observed in the presence of non-averaged structural elements. Molten-globule structures typically show an absence or reduction of signals in the near-UV region because of their time-averaged fluctuations. In contrast, native-like structures display more intense absorptions in this region due to their specific interhelical packing. Figure 3 shows the near-UV/CD spectra of the second-generation caviteins. The 1GS2 and 4GS2 caviteins show the most reduced signals in the near-UV region, which indicates the presence of averaged structural elements near the cavitand. The linker in the 1GS2 cavitein may be too short to allow specific side-chain interactions, thereby giving rise to a structure with molten-globule character. The longer linker in the 4GS2 cavitein may render the structure too flexible, also resulting in a molten-globule structure. It is important to note that the near-UV/CD data depends on the distance between the helices and the cavitand chromophore, and therefore this data may only be useful for the species with the shorter linkers (i.e. caviteins with one or two Gly linkers). The 2GS2 cavitein shows the most enhanced signal in the near-UV region of the CD spectra relative to all the caviteins in both the first-[14] and second-generation series, suggesting it is less dynamic and is packed more efficiently near the cavitand chromophore.

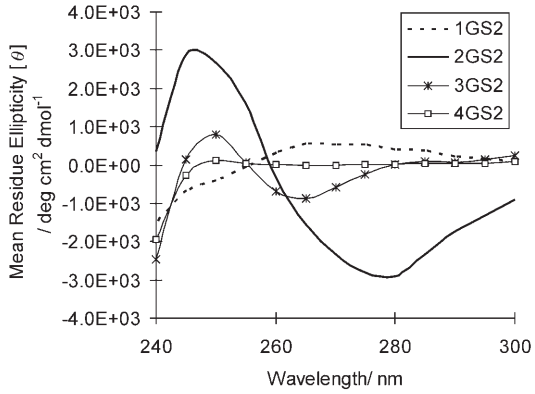

Figure 3. Near-UV/CD spectra of the caviteins. Samples are 40 μM in pH 7.0, 50 mM phosphate buffer at 25 °C.

Effect of guanidine hydrochloride: The stabilities of the caviteins were assessed by using the denaturant guanidine hydrochloride (GuHCl).[22] Figure 4 shows the denaturation curves of the caviteins and the non-templated control peptide **6**. GuHCl easily denatured peptide **6**, but barely denatured the four-helix bundle caviteins.

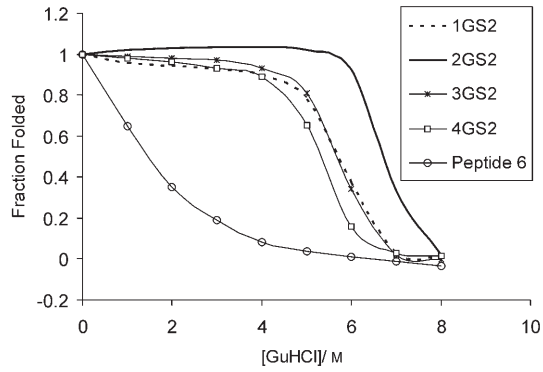

Figure 4. GuHCl-induced denaturation curve of the caviteins. The high 40 μM and low 4 μM concentration samples gave overlapping curves, and therefore only the data for the high concentration sample is shown. Error bars are ±5%, but omitted for clarity and explained in the Experimental Section.

It is apparent that the caviteins with varying linker lengths possess different stabilities. A crude way to assess the stabilities of the proteins is to visually observe the concentration of GuHCl required to unfold half the protein, $[GuHCl]_{1/2}$. A more accurate method for determining the stabilities is to calculate the free energies of folding using linear extrapolation methods.[23] Table 2 presents the GuHCl-induced denaturation data for the caviteins. The resulting free energies in Table 2 assumes that the unfolding transition is a reversible, two-state process, and that the free energy of unfolding varies linearly with the concentration of the denaturant (see Experimental Section). The *m* values in Table 2 correspond

Table 2. GuHCl-induced denaturation data.

Cavitein	$[GuHCl]_{1/2}$ [M]	*m* [kcal mol^{-1} M^{-1}]	$\Delta G^{o}_{H_2O}$ [kcal mol^{-1}]
1GS2	5.4±0.1	−1.4±0.1	−8.3±0.3
2GS2	6.9±0.1	−2.1±0.1	−14.1±0.7
3GS2	5.3±0.1	−1.8±0.1	−10.6±0.3
4GS2	4.9±0.1	−1.5±0.1	−7.9±0.3

to the observed free energy of folding as a function of the [GuHCl], and are comparable to those of natural proteins.[24] High *m* values have been associated with cooperativity, and high cooperativity has been related to native-like character.[25] The 1GS2 and 4GS2 caviteins were found to be the least stable toward the denaturant, indicating that the optimal linker lies somewhere in between these two linker lengths. The 2GS2 cavitein was found to be the most stable species and it has the largest *m* value of the second generation series, which suggests that it is the most native-like. It also has a more negative $\Delta G^{o}_{H_2O}$ value and a larger *m* value relative to the monomeric caviteins (i.e., 2 and 3 Gly variants) of the first-generation series.[14] The calculations for the free energy of folding should be interpreted with some caution, because there is no proof for assuming that the unfolding varies linearly with denaturant concentration. At high concentrations, this assumption may fail and introduce errors. Furthermore, errors substantially increase as the length of extrapolation is expanded. In other words, larger errors are incorporated when the denaturation midpoint is higher.[23] All the caviteins demonstrated concentration-independent curves, which indicates that these proteins exist as monomers, at least at the point of denaturation. The presence of GuHCl may have disrupted self-aggregation, should any exist. Therefore, sedimentation equilibria studies, in the absence of the denaturant, were carried out in order to determine the oligomeric state of the caviteins in buffer alone.

Oligomeric state: Sedimentation equilibria studies were performed by using an analytical ultracentrifuge to determine the molecular weight of the various caviteins in solution. Three different concentrations and three different rotor speeds were employed for each protein. From the experiments, the 1GS2 exists in a monomer-dimer equilibrium, the 3GS2 cavitein is predominantly dimeric, and the 2GS2 and 4GS2 caviteins exist as monomers. One Gly may be causing strain within the packing, thereby exposing the hydrophobic core and resulting in a monomer–dimer equilibrium. The two-Gly linker is the optimal length to obtain a monomeric species. The 4GS2 cavitein also exists as a monomer, which shows that the linker allows sufficient flexibility to prevent self-association, although its native-like character and stability could be sacrificed. The 3GS2 cavitein exists as a dimer, but this is interpreted with caution, since it behaves anomalously (see ^{1}H NMR spectroscopy and N-H/D exchange sections).

^{1}H NMR spectra: Generally, ^{1}H NMR spectroscopy can be used to determine the extent of a protein's native-like char-

acter. Analysis of ^{1}H NMR linewidths and chemical-shift dispersion can be used to determine conformational heterogeneity. Sharp, well-dispersed signals are indicative of a native-like protein,[26] and broad, less-dispersed peaks are indicative of a molten-globule structure.[27] Figure 5 shows the

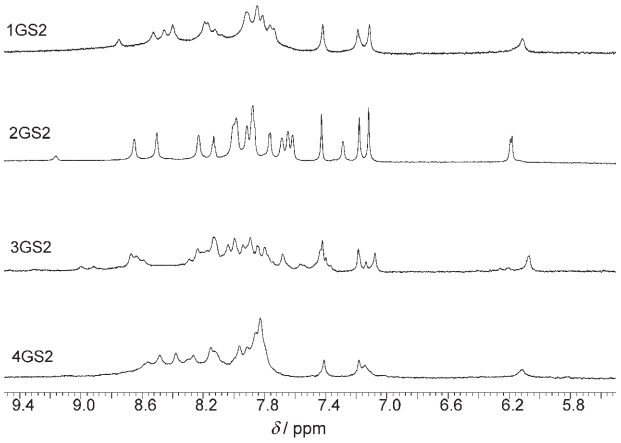

Figure 5. Expanded amide regions of the ^{1}H NMR spectra of the caviteins in pH 7.0, 50 mM phosphate buffer with 10% D_2O at 25°C and 600 MHz.

expanded amide region of the caviteins studied here. The 2GS2 cavitein contains the sharpest and most well-dispersed signals, which indicates the presence of a well-organised hydrogen-bond network of the amide protons. In addition, the cavitand signal at around $\delta = 6.1$ ppm, which corresponds to H_{out} (see Scheme 2) appears as a doublet for the 2GS2 cavitein, whereas it appears as a broad singlet for the rest of the caviteins. The H_{out} signal should be a doublet because it is *J*-coupled to the H_{in} proton. Since the 2GS2 cavitein is the only species that yields a resolved doublet, it is likely that the packing within the core of this protein is the most efficient, and hence the most native-like. The 1GS2 and 4GS2 caviteins show broad, less-dispersed signals, indicating a lack of conformational specificity, consistent with the other experimental data. The shorter linker in the 1GS2 cavitein may distort the helices by restricting them near the cavitand template. The long linkers of 4GS2 may evade aggregation, but excess flexibility compromises its native-like structure. The 3GS2 cavitein was not analysed further because its ^{1}H NMR spectrum changes over time in solution. Depending on when the measurements were taken after sample preparation for the 3GS2 cavitein, certain signals decreased and additional signals appeared (more explanation in the N-H/D exchange section). Next, Figure 6 shows the aliphatic region of the spectra. Again, the 1GS2 and 4GS2 caviteins show the least dispersed signals, and the 2GS2 cavitein displays the sharpest, most dispersed signals in its spectrum, particularly around $\delta = 0.8$ ppm, which represents the δ methyl protons of the Leu residues in the hydrophobic core.

2D ^{1}H NMR spectra: 2D ^{1}H NMR spectroscopy is a useful tool for investigating the tertiary structure of proteins[28] and

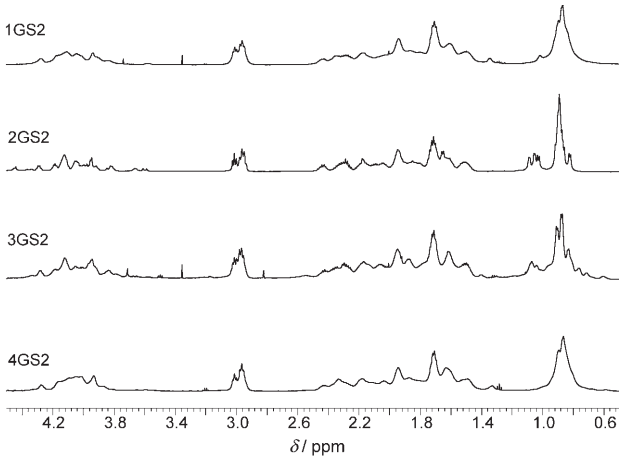

Figure 6. Expanded aliphatic regions of the ^{1}H NMR spectra of the caviteins in pH 7.0, 50 mM phosphate buffer with 10% D_2O at 25°C and 600 MHz.

assigning proton resonances.[29] Here, 2D correlation spectroscopy (COSY), total correlation spectroscopy (TOCSY) and nuclear Overhauser enhancement spectroscopY (NOESY) were used to assign the proton signals in the amide region. The 2D ^{1}H NMR spectra are included in the Supporting Information. Figure 7 shows the assigned 1D

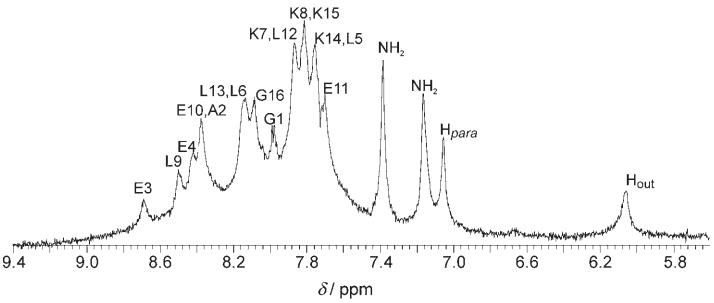

Figure 7. 500 MHz 1D ^{1}H NMR spectrum of the 1GS2 cavitein in 50 mM acetate buffer, pH 4.62, with 10% D_2O at 20°C, expanded in the amide region. Signals are labelled based on the resonance assignments from the 2D NMR spectra (see Supporting Information).

^{1}H NMR spectrum of the 1GS2 cavitein and Figure 8 shows the assigned 1D ^{1}H NMR spectrum of the 2GS2 cavitein. The resonances were not assigned for the 3GS2 and 4GS2 caviteins owing to the time-dependent behaviour and poor dispersion of the signals, respectively. This study reports the first resonance assignments of the cavitein systems.

N-H/D exchange experiments: Hydrogen/deuterium exchange experiments have been used to assess the dynamic behaviour of proteins.[30,31] The experiments are performed and evaluated on the basis that well-defined, native-like proteins have more protected amide protons than molten globules. The extent of solvent accessibility is expressed as a protection factor (*P*), which is dependent on temperature and pH. Typically backbone amide protons of native-like proteins have protection factors that range from 10^4 to 10^8,[32]

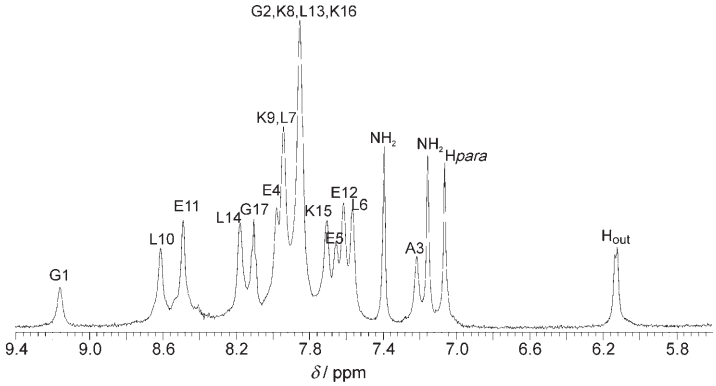

Figure 8. 500 MHz 1D ^{1}H NMR spectrum of the 2GS2 cavitein in 50 mM acetate buffer, pH 4.62, with 10% D_2O at 20°C, expanded in the amide region. Signals are labelled based on the resonance assignments from the 2D NMR spectra.

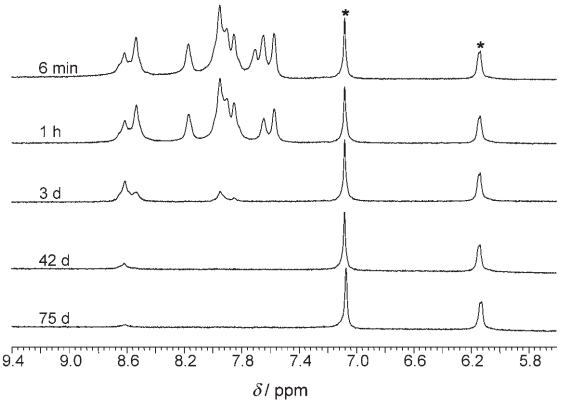

Figure 9. Stack plot of 500 MHz 1D ^{1}H NMR spectra of the 2GS2 cavitein in 50 mM deuterated acetate buffer, pD 5.02 at 20°C. The * represents the non-exchangeable cavitand signals.

whereas molten-globule structures have protection factors that range from 10 to 10^3.[33] The exchange rates of the caviteins were studied at 20°C, pD 5.02. Table 3 presents the first-order exchange rates and protection factors from the N-H/D exchange data, which is based on the amide-proton signal that remained the longest. From the 2D NMR resonance assignments, it was determined that the last amide proton to disappear from both the 1GS2 and 2GS2 caviteins was the central non-polar residue of the sequence (i.e., L9 for the 1GS2 cavitein and L10 for the 2GS2 cavitein). Overall, the 2GS2 cavitein displays the highest protection factor, consistent with a native-like protein. Figure 9 shows the 1D ^{1}H NMR stack plot of the 2GS2 cavitein during N-H/D exchange.

Table 3. N-H/D exchange data of the caviteins in 50 mM deuterated acetate buffer, pD 5.02 at 20°C. Exchange data could not be determined for the 3GS2 cavitein, since the cavitand signal of this species changed over time.

Cavitein	First-order exchange rate [h^{-1}]	Half-life [h]	Protection factor
1GS2	1.4 ± 0.4	0.50 ± 0.08	1.6 ± 0.2
2GS2	$(4\pm1)\times10^{-3}$	$1.9\pm0.7\times10^{-2}$	$(6\pm1)\times10^{4}$
3GS2	N/A	N/A	N/A
4GS2	3.5 ± 0.8	0.20 ± 0.04	$(6.0\pm0.8)\times10^{1}$

For the 3GS2 cavitein, the cavitand signals decreased over time, which should have stayed constant, and new signals appeared around the cavitand signals (see Supporting Information). The 1GS2 and 4GS2 caviteins possess protection factors that are characteristic of molten-globule structures. Compared to the monomeric caviteins in the first-generation series,[34] the 2GS2 cavitein has a protection factor that is tenfold higher than the rest. The cavitand signals that were used to normalise the amide-proton signals remained constant for the rest of the proteins except for the 3GS2 cavitein, and thus, protection factors could not be calculated for this species.

The longest lasting amide proton (i.e., the middle non-polar residue) appears to play an important role in maintaining the overall protein structure. Work has been carried out to study the context dependence of the non-polar residues in the four-helix caviteins, which also revealed that the central non-polar residue is the most important position in maintaining a stable, well-defined cavitein.[35]

ANS binding studies: 1-Anilinonaphthalene-8-sulfonate (ANS) is a hydrophobic dye that is used to detect the presence of molten-globule proteins.[36] ANS preferentially binds to the molten-globule states due to their fluctuating structures. Thus, ANS binding studies have been used to determine the extent of native-like character here.[7] Figure 10 displays the fluorescence emission spectra of ANS in the presence of the second-generation caviteins. The caviteins only weakly bind ANS; however, this does not necessarily indicate the absence of molten-globule structures as seen from the near-UV/CD and ^{1}H NMR spectra. In general, the 1GS2 cavitein consistently bound the most ANS and the 2GS2 cavitein bound the least amount of ANS; these results agree with the near-UV/CD spectra, sedimentation equili-

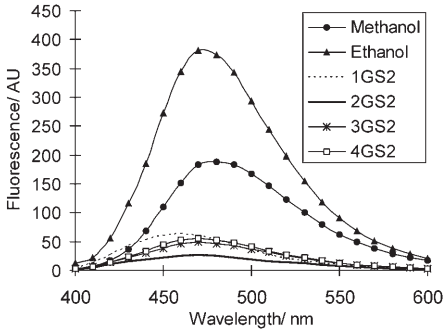

Figure 10. Fluorescence emission spectra of 2 μM ANS in the presence of 100% methanol, 95% ethanol and 50 μM of each cavitein: 1GS2, 2GS2, 3GS2 and 4GS2 in 50 mM phosphate buffer, pH 7.0 at 25°C. Error bars are ±5%, but omitted for clarity and explained in the Experimental Section.

bria data and ^{1}H NMR spectra. The non-linked reference peptide **6** did not bind any ANS regardless of sample concentration. The fluorescence intensity remained on the baseline throughout the scan (not shown).

Computer modelling: The second-generation caviteins were studied by molecular dynamics (MD) simulations. The methods used here were described previously for the study of the first-generation cavitein series by MD stimulations.[37] Three sets of simulations were performed for up to 20 ns in order to minimise bias toward the starting configuration. Ramachandran plots were generated and the secondary structure was analysed. All four of the caviteins in the second-generation series were found to be α-helical, which agrees with the CD spectra. The conformational specificity was characterised in terms of the structural spread encountered during the course of the simulation.[37] A representative cluster obtained for the 2GS2 cavitein is shown in Figure 11. The

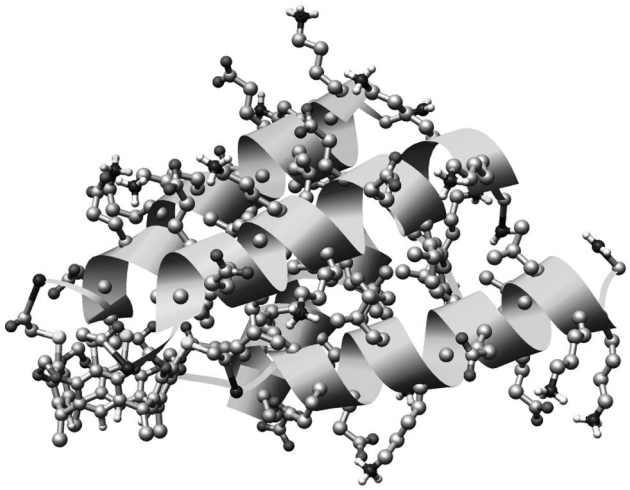

Figure 11. Representative cluster of the 2GS2 cavitein.

image was generated using the Chimera program.[38] The helices of the 2GS2 cavitein are tilted with respect to the cavitand template, which may explain some of its distinctive properties observed experimentally. For example, the 2GS2 exists as a stable monomer (by GuHCl-induced denaturation studies and sedimentation equilibria studies), because the tilt of the helices could increase the burial of the non-polar residues. The tilt may also facilitate improved packing between the helices, which may explain the 2GS2 cavitein's high degree of native-like character. However, from the study of the first-generation cavitein series by MD, the one-Gly variant (1GS1) was also found to possess tilted helices with respect to the cavitand,[37] although it was found to exist as a dimer by sedimentation equilibria studies.[14] This contrast can be attributed to the difference within the inter-helical packing. For the 2GS2 cavitein, the tilt increased the burial of the non-polar residues, reducing exposure of the hydrophobic core; however, for the 1GS1 cavitein, two of the four helices in the tilt were solvent exposed, suggesting that the dimerisation could occur at this exposed interface.[37] It is important to note that the simulation results are not always accurate due to assumptions made in the force field and calculations, as well as due to time limitations. Nevertheless, results obtained from the simulations can help complement the experimental results and allow us to better comprehend the behaviour of the caviteins.

Conclusions

An objective of de novo design and synthesis is to evaluate the features that influence the structure and ultimately the function of a protein. The success or failure of a design tests the underlying concepts and principles involved in folding. Using a template approach has proven to be a useful tool in understanding protein structure, because it allows for the regulation of certain features such as orientation and number of helices in a bundle. Our group examined the effect of the linker length in depth by using a cavitand as a template. From the first-generation cavitein studies, using a peptide sequence designed to link the hydrophobic/hydrophilic interface, it was determined that two to three Gly residues were necessary to obtain a well-defined structure.[14] From the second-generation cavitein studies presented in this paper, it is clear that two Gly residues are optimal in obtaining a native-like protein when the peptides are linked closer to the hydrophobic face. Comparing the caviteins in both generations, the two-Gly variant of the second generation series (i.e., 2GS2 cavitein) displays the most characteristics of a native-like protein. Linking the peptides closer to the hydrophobic face improved the packing between the helices, and hence its native-like properties. The 2GS2 cavitein also displays similar structural specificity to known native-like de novo proteins.[5,28] Molecular dynamics simulations show that the unique properties of the 2GS2 cavitein could be a result of tilted helices with respect to the cavitand template.

Although the goal of the protein folding problem is to learn about the relationship between the amino acid sequence and tertiary structure of the proteins, we are also interested in learning about the helical bundle systems. From the 2D ^{1}H NMR spectra, we were able to assign the amide protons, which was a first for the caviteins. Together with the resonance assignments of the amide protons and N-H/D exchange data, it was determined that the middle non-polar Leu residue was the last amide proton to exchange with the solvent, indicating that the ends of the bundle are more dynamic than the centre. With improved understanding of how the different forces interact to influence the folded protein, it should be possible to direct the design of more complex caviteins with function. De novo proteins have been designed to mimic ion channels,[39] receptor binding proteins,[40] antiviral agents,[41] enzymes[42,43] and artificial redox systems.[43,44]

Experimental Section

Cavitand synthesis: The synthesis of the cavitand template has been described previously.[17]

General: All chemicals used for peptide and cavitein synthesis were reagent grade. The peptides and caviteins were purified by reversed-phase HPLC by using a gradient composed of helium-sparged HPLC grade acetonitrile (0.05% TFA), and filtered, helium-sparged deionised water (0.1% TFA) at a flow rate of 10 mL min^{-1} on a Phenomenex Selectosil C_{18} column (250×22.5 mm, 10 μm particle size, 300 Å pore size). The purity of the peptides and caviteins were checked by analytical reversed-phase HPLC at a flow rate of 1.0 mL min^{-1} on a Waters Delta Pak C_{18} column (300 mm, 3.9 mm, 15 μm, 300 Å). The molecular weight of the peptides and proteins were determined by a Bruker Biflex IV MALDI mass spectrometer with saturated cinammic acid as the matrix.

Peptide synthesis: All peptides were synthesised on an Applied Biosystems (ABI) 431A automated peptide synthesiser by using standard solid-phase methods and Fmoc/*t*Bu chemistry. Rink resin was used to afford peptides with C-terminal amides.[45] All solvents and reagents were purchased from Advanced Chem Tech with the exception of DMF, piperidine and the activating reagents, which were purchased from Aldrich.

Peptide 1: The peptide on the resin (≈700 mg, ≈350 mg peptide, 0.187 mmol) was treated with chloroacetyl chloride (90 μL, 1.12 mmol, 6 equiv) and DIPEA (195 μL, 1.12 mmol, 6 equiv) in DMF (5 mL) for 1 h at RT under N_2. After cleavage from the resin and of the protecting groups from the peptides, purification and lyophilisation, a white solid was obtained (130 mg, 28%). MS: *m*/*z*: 1875 $[M+H]^+$

Peptide 2: The peptide on the resin (≈700 mg, ≈350 mg peptide, 0.181 mmol) was treaced with chloroacetyl chloride (74 μL, 0.93 mmol, 6 equiv) and DIPEA (162 μL, 0.93 mmol, 6 equiv) in DMF (5 mL) for 1 h at RT under N_2. After cleavage from the resin and of the protecting groups from the peptides, purification and lyophilisation, a white solid was obtained (155 mg, 32%). MS: *m*/*z*: 1932 $[M+H]^+$

Peptide 3: The peptide on the resin (≈600 mg, ≈300 mg peptide, 0.151 mmol) was treated with chloroacetyl chloride (72 μL, 0.91 mmol, 6 equiv) and DIPEA (159 μL, 0.91 mmol, 6 equiv) in DMF (5 mL) for 1 h at RT under N_2. After cleavage from the resin and of the protecting groups from the peptides, purification and lyophilisation, a white solid was obtained (110 mg, 22%). MS: *m*/*z*: 1989 $[M+H]^+$

Peptide 4: The peptide on the resin (≈600 mg, ≈300 mg peptide, 0.147 mmol) was treated with chloroacetyl chloride (70 μL, 0.88 mmol, 6 equiv) and DIPEA (154 μL, 0.88 mmol, 6 equiv) in DMF (5 mL) for 1 h at RT under N_2. After cleavage from the resin and of the protecting groups from the peptides, purification and lyophilisation, a white solid was obtained (180 mg, 24%). MS: *m*/*z*: 2046 $[M+H]^+$

Peptide 5: The peptide on the resin (≈700 mg, ≈350 mg peptide, 0.192 mmol) was treated with chloroacetyl chloride (91 μL, 1.14 mmol, 6 equiv) and DIPEA (200 μL, 1.14 mmol, 6 equiv) in DMF (5 mL) for 1 h at RT under N_2. After cleavage from the resin and of the protecting groups from the peptides, purification and lyophilisation, a white solid was obtained (141 mg, 31%). MS: *m*/*z*: 1818 $[M+H]^+$

Peptide 6: The last cycle in the synthesis of the reference peptide involved acetylating the N terminus by using 10% acetic anhydride (2 mL) in NMP (1 mL) and stirred at RT for 1 h. The resin and protecting groups were cleaved from the peptide by treatment with 95% TFA in water for 2 h. After purification and lyophilisation, the afforded peptide was a white solid (15 mg, 20%). MS: *m*/*z*: 1783 $[M+H]^+$

Cavitein synthesis: The caviteins were synthesised by reacting the cavitand template with the peptides from above under basic conditions.

1GS2: DIPEA (2.4 μL, 14 μmol, 10 equiv) was added to a solution of the cavitand template (1.0 mg, 1.4 μmol, 1 equiv) and peptide **1** (20 mg, 11 μmol, 8 equiv) in degassed DMF (1 mL), and the reaction was stirred for 5 h at RT under N_2. The crude reaction mixture was evaporated in vacuo and purified by reversed-phase HPLC to afford the cavitein as a white solid after lyophilisation (6 mg, 54%). MS: *m*/*z*: 8069.5 $[M+H]^+$

2GS2: The same procedure described for 1GS2 was employed but with peptide **2** (21 mg, 11 μmol, 8 equiv) to afford a white solid (5.6 mg, 49%). MS: *m*/*z*: 8298.5 $[M+H]^+$

3GS2: The same procedure described for 1GS2 was employed but with peptide **3** (22 mg, 11 μmol, 8 equiv) to afford a white solid (4 mg, 34%). MS: *m*/*z*: 8527.2 $[M+H]^+$

4GS2: The same procedure described for 1GS2 was employed but with peptide **4** (23 mg, 11 μmol, 8 equiv) to afford a white solid (7 mg, 57%). MS: *m*/*z*: 8755.1 $[M+H]^+$

Circular dichroism (CD) spectroscopy: The CD spectra were recorded on a JASCO J-710 spectropolarimeter at 25°C. The background correction was performed by substracting the scan of 50 mM pH 7.0 phosphate buffer from the sample scan. Three scans were taken and averaged for every sample. Quartz cuvettes of either 1 mm or 1 cm path lengths were used to hold the samples to make sample concentrations of 40 μM and 4 μM, respectively. The instrument was routinely calibrated with $[D_{10}]$camphorsulfonic acid. The raw CD spectra were normalised to mean residue ellipticity $[\theta]$ at 222 nm using Equation (1) in which θ_{obs} is the ellipticity measured in millidegrees, *l* is the cell pathlength in cm, *c* is the concentration in M, and *n* is the number of residues in the cavitein.

$$[\theta]_{222} = \theta_{obs}/10\,l\,c\,n \quad (1)$$

The errors represent the standard deviation of each point and were found to be ±5%. The concentrations of the caviteins were determined by using the Bradford assay[46] and had errors of ±10%.

Denaturation experiments: The GuHCl-induced denaturation experiments were carried out on the CD spectrometer with a solution of 8.0 M GuHCl. The sample concentrations were 40 μM and 4 μM, and prepared in a 1 cm or 1 mm quartz cuvette, respectively. To obtain the most concentrated 8.0 M solution of GuHCl, the protein was directly dissolved in the 8.0 M stock solution. The other samples of lower GuHCl concentrations were prepared by appropriately diluting the samples with pH 7.0, 50 mM phosphate buffer from 0 M to 8.0 M GuHCl in 0.25 M increments of the denaturant. The samples were typically prepared a day ahead and vortexed before measurement. Three different scans of three separately prepared samples were taken and the errors were found to be within ±5%. The fraction folded was determined from dividing the $[\theta]_{222}$ at a certain concentration of GuHCl with the $[\theta]_{222}$ of the completely folded protein.

The stabilities of the caviteins were determined using the linear extrapolation method,[23] which assumes that the folding/unfolding of a protein is a reversible, two state process: U⇄N in which N is the folded native-state of the protein, and U is the fully unfolded state of the protein. This method also assumes that the folding free energy is linearly dependent on the concentrations of GuHCl. Equation (2) relates the observed free energy of folding, ΔG^o_{obs} with the free energy of folding in the absence of the denaturant, $\Delta G^o_{H_2O}$.

$$\Delta G^o_{obs} = \Delta G^o_{H_2O} - m[\mathrm{GuHCl}] \quad (2)$$

In Euqation (2) *m* is the change in ΔG^o_{obs} with respect to the concentration of GuHCl. At a particular denaturant concentration, ΔG^o_{obs} can be calculated according to Equation (3)in which *R* is the universal gas constant, *T* is the temperature and K_{obs} is the equilibrium constant for folding [Eq. (4)].

$$\Delta G^o_{obs} = -R\,T\ln K_{obs} \quad (3)$$

$$K_{obs} = \frac{[N]}{[U]} = e^{(-\Delta G^o_{obs}/RT)} = e^{((-\Delta G^o_{H_2O} - m[\mathrm{GuHCl}])/RT)} = \frac{f_N}{f_U} = \frac{f_N}{(1-f_N)} \quad (4)$$

In Equation (4) f_N and f_U are the fraction of folded and the fractio of unfolded protein, respectively. The parameter f_N can be determined using Equation (5).

$$f_N = \frac{e^{((-\Delta G^o_{H_2O} - m[GuHCl])/RT)}}{[1 + e^{((-\Delta G^o_{H_2O} - m[GuHCl])/RT)}]} \quad (5)$$

For proteins with high stability, the post-transitional baseline may be difficult to approximate at high concentrations of GuHCl, therefore Equation (6)[47] is used in which θ_{obs} is the ellipticity at 222 nm at a given GuHCl concentration, θ_N is the ellipticity of the fully folded state, θ_U is the ellipticity of the unfolded state, and a is a constant.

$$\theta_{obs} = \theta_N(f_N)(1 - a[GuHCl]) + \theta_U(1 - f_N) \quad (6)$$

The values for, θ_U, $\Delta G^o_{H_2O}$, m and a were determined by non-linear least-squares analysis by using KaleidaGraph 3.08 (Synergy Software). The value of θ_N was normalised to 0.9999 and θ_U was set to 0.0001. The errors reported are calculated from this program.

Analytical ultracentrifuge: Sedimentation equilibria studies were carried out to determine the oligomeric state of the caviteins by using a temperature-controlled Beckman Coulter Optima XL-1 analytical ultracentrifuge with an AN60 Ti 4-hole rotor. Different initial concentrations of 20, 40 and 60 μM solutions were made up with 50 mM pH 7.0 phosphate buffer. To each sample, KCl (0.08 M) was added. The samples were loaded with 125 μL of cavitein solution and 135 μL of reference solution into ultracentrifuge cells containing Epon six-channel centrepieces with 12 mm pathlength quartz windows. Data were collected at 20 °C at rotor speeds of 27000, 35000, and 40000 rpm until equilibrium was reached (29–35 h). Scans were detected by UV at a wavelength of 270 nm. The partial specific volumes of the caviteins were calculated based on their amino acid composition.[48] The solution density of the samples in aqueous buffer was estimated to be 1.000 g mL^{-1}. The data were analysed by using a non-linear least-squares analysis.[49] The data were initially fit to a single, ideal species.[50] In cases in which the data did not fit well to a single ideal species, best fits were made using a self-associating model.[50] Raw data of the fits are included in the Supporting Information.

NMR spectroscopy:[51] The 1D ^{1}H NMR spectra were obtained on a 600 MHz Varian Unity Inova NMR spectrometer at 25 °C. The cavitein samples were prepared by dissolving the protein in 45 mM phosphate buffer (90:10 H_2O/D_2O) at pH 7.0. The final concentrations of all the caviteins were 1.5 mM. The data were processed by using MestReC Version 2.3.

To obtain the 2D ^{1}H NMR spectrum of the 2GS2 cavitein sample, a 500 MHz Varian Unity instrument at 20 °C was used. The 1GS2 cavitein sample was run on a 600 MHz Varian Unity Inova at 20 °C. The concentration of the 2GS2 cavitein sample was 2 mM and that of the 1GS2 cavitein sample was 1.1 mM. The samples were dissolved in 45 mM acetate buffer (90:10 H_2O/D_2O) at pH 4.62. The 2D spectra were processed by using NMRpipe, and polynomial baseline corrections were carried out. The spectra were calibrated to the water signal at $\delta = 4.78$ ppm. The resonance assignments were assisted by using NMRView.

The N-H/D exchange experiments were run on a 500 MHz Varian Unity at 20 °C. The samples were prepared by dissolving the caviteins in 50 mM acetate buffer at pH 4.62, and lyophilising these samples. The experiment was initiated by the addition of 100 % D_2O. The sample concentrations were 2.2 mM for the 1GS2 cavitein, 1.9 mM for the 2GS2 cavitein, 1.9 mM for the 3GS2 cavitein and 1.9 mM for the 4GS2 cavitein. The pD was corrected for isotope effects.[52] The reference spectrum consisted of each cavitein in 45 mM acetate buffer (90:10 H_2O/D_2O) at 20 °C. The peak heights were normalised with the non-exchangeable proton, H_{out} (near $\delta = 6$ ppm) of the cavitand template. The first-order rate could not be determined for the 3GS2 cavitein, since the H_{out} signal changed over time. The protection factor, P was calculated using Equation (7),[32] and was based on the last amide proton to disappear for each cavitein.

$$P = k_{int}/k_{ex} \quad (7)$$

In Equation (7) k_{int} is the intrinsic exchange rate[30] of an unprotected proton and k_{ex} is the first order exchange rate of the amide proton in question. The values in Table 3 correspond to the chemical shift of the last amide proton to disappear during exchange (i.e., middle Leu). The calculated data are the averages of three estimates at three different times. The listed errors represent the standard deviation of the estimates.

ANS binding studies: ANS fluorescence spectra were measured on a Varian CARY Eclipse at 25 °C. A quartz cell with a 10 mm pathlength was used to hold the samples. All samples contained 2 μM ANS in 50 mM phosphate buffer at pH 7.0, and either 50 μM of the cavitein, 95 % ethanol, or 100 % HPLC grade methanol. The excitation wavelength was set to 370 nm and the emission was recorded between 400 and 600 nm. The error bars were calculated from the standard deviation of three separate runs and were found to be ±5 %.

Acknowledgement

We would like to thank the Natural Sciences and Engineering Research Council of Canada (J.C.S.) for financial support and the University of British Columbia for financial awards (ESS). A special thanks to M. Okon for acquiring the ^{1}H NMR spectra and sharing his NMR knowledge. We would like to acknowledge the Centre for Biothermodynamics and support from the Michael Smith Foundation for Health Research for the data collected on the analytical ultracentrifuge. The molecular graphics image was produced by using the UCSF Chimera package from the Resource for Biocomputing, Visualisation, and Informatics at the University of California, San Francisco (supported by NIH P41 RR-01081).

[1] a) W. F. DeGrado, C. M. Summa, V. Pavone, F. Nastri, A. Lombardi, *Annu. Rev. Biochem.* **1999**, *68*, 779–819; b) R. B. Hill, D. P. Raleigh, A. Lombardi, W. F. DeGrado, *Acc. Chem. Res.* **2000**, *33*, 745–754; c) L. Baltzer, H. Nilsson, J. Nilsson, *Chem. Rev.* **2001**, *101*, 3153–3163.

[2] a) M. Mutter, S. Vuilleumier, *Angew. Chem.* **1989**, *101*, 551–571; *Angew. Chem. Int. Ed. Engl.* **1989**, *28*, 535–554; b) M. Mutter, G. G. Tuchscherer, C. Miller, K. H. Altmann, R. I. Carey, D. F. Wyss, A. M. Labhardt, J. E. Rivier, *J. Am. Chem. Soc.* **1992**, *114*, 1463–1470; c) G. Tuchscherer, M. Mutter, *J. Biotechnol.* **1995**, *41*, 197–210; d) G. Tuchscherer, M. Mutter, *J. Pept. Sci.* **2005**, *11*, 278–282.

[3] a) T. Sasaki, E. T. Kaiser, *J. Am. Chem. Soc.* **1989**, *111*, 380–381; b) M. R. Ghadiri, C. Soares, C. Choi, *J. Am. Chem. Soc.* **1992**, *114*, 4000–4002; c) J. Brask, J. M. Dideriksen, J. Nielsen, K. J. Jensen, *Org. Biomol. Chem.* **2003**, *1*, 2247–2252; d) K. Tsukamoto, H. Ohishi, N. Maezaki, T. Tanaka, T. Ishida, *ChemBioChem* **2006**, *7*, 1559–1562.

[4] a) S. P. Ho, W. F. DeGrado, *J. Am. Chem. Soc.* **1987**, *109*, 6751–6758; b) J. J. Osterhout, Jr., T. Handel, G. Na, A. Toumadje, R. C. Long, P. J. Connolly, J. C. Hoch, W. C. Johnson, Jr., D. Live, W. F. DeGrado, *J. Am. Chem. Soc.* **1992**, *114*, 331–337.

[5] D. P. Raleigh, S. F. Betz, W. F. DeGrado, *J. Am. Chem. Soc.* **1995**, *117*, 7558–7559.

[6] a) C. P. Hill, W. F. DeGrado, *Structure* **2000**, *8*, 471–479; b) R. B. Hill, J. K. Hong, W. F. DeGrado, *J. Am. Chem. Soc.* **2000**, *122*, 746–747.

[7] S. Roy, G. Ratnaswamy, J. A. Boice, R. Fairman, G. McLendon, M. H. Hecht, *J. Am. Chem. Soc.* **1997**, *119*, 5302–5306.

[8] M. H. Hecht, A. Das, A. Go, L. H. Bradley, Y. Wei, *Protein Sci.* **2004**, *13*, 1711–1723.

[9] A. D. Nagi, K. S. Anderson, L. Regan, *J. Mol. Biol.* **1999**, *286*, 257–265.

[10] B. Simons, D. Scholl, T. Cyr, M. A. Hefford, *Protein Pept. Lett.* **2001**, *8*, 89–96.

[11] a) A. K. Wong, M. P. Jacobsen, D. J. Winzor, D. P. Fairlie, *J. Am. Chem. Soc.* **1998**, *120*, 3836–3841; b) H. Li, L. X. Wang, *Org. Biomol. Chem.* **2003**, *1*, 3507–3513.
[12] J. R. Moran, S. Karbach, D. J. Cram, *J. Am. Chem. Soc.* **1982**, *104*, 5826–5828.
[13] B. C. Gibb, A. R. Mezo, J. C. Sherman, *Tetrahedron Lett.* **1995**, *36*, 7587–7590.
[14] A. R. Mezo, J. C. Sherman, *J. Am. Chem. Soc.* **1999**, *121*, 8983–8994.
[15] W. F. DeGrado, Z. R. Wasserman, J. D. Lear, *Science* **1989**, *243*, 622–628.
[16] R. Aurora, R. Srinivasan, G. D. Rose, *Science* **1994**, *264*, 1126–1130.
[17] B. C. Gibb, A. R. Mezo, A. S. Causton, J. R. Fraser, F. C. S. Tsai, J. C. Sherman, *Tetrahedron* **1995**, *51*, 8719–8732.
[18] P. Timmerman, W. Verboom, D. N. Reinhoudt, *Tetrahedron* **1996**, *52*, 2663–2704.
[19] B. V. B. Reddy, T. L. Blundell, *J. Mol. Biol.* **1993**, *233*, 464–479.
[20] a) R. W. Woody, *Biopolymers* **1978**, *17*, 1451–1467; b) A. Chakrabartty, T. Kortemme, S. Padmanabhan, R. L. Baldwin, *Biochemistry* **1993**, *32*, 5560–5565.
[21] F. Offredi, F. Dubail, P. Kischel, K. Sarinski, A. S. Stern, C. Van de Weerdt, J. C. Hoch, C. Prosperi, J. M. Francois, S. L. Mayo, J. A. Martial, *J. Mol. Biol.* **2003**, *325*, 163–174.
[22] C. N. Pace, *Methods Enzymol.* **1986**, *131*, 266–280.
[23] M. M. Santoro, D. W. Bolen, *Biochemistry* **1988**, *27*, 8063–8068.
[24] F. Ahmad, C. C. Bigelow, *Biopolymers* **1986**, *25*, 1623–1633.
[25] W. F. DeGrado, D. P. Raleigh, T. Handel, *Curr. Opin. Struct. Biol.* **1991**, *1*, 984–993.
[26] S. Roy, K. J. Helmer, M. H. Hecht, *Folding Des.* **1997**, *2*, 89–92.
[27] A. T. Alexandrescu, P. A. Evans, M. Pitkeathly, J. Baum, C. M. Dobson, *Biochemistry* **1993**, *32*, 1707–1718.
[28] C. P. Hill, W. F. DeGrado, *J. Am. Chem. Soc.* **1998**, *120*, 1138–1145.
[29] Y. Kuroda, T. Nakai, T. Ohkubo, *J. Mol. Biol.* **1994**, *236*, 862–868.
[30] S. W. Englander, N. W. Downer, H. Teitelbaum, *Annu. Rev. Biochem.* **1972**, *41*, 903–924.
[31] T. Raschke, S. Marqusee, *Curr. Opin. Biotechnol.* **1998**, *9*, 80–86.
[32] M. F. Jeng, S. W. Englander, G. A. Elove, J. A. Wang, H. Roder, *Biochemistry* **1990**, *29*, 10433–10437.
[33] F. M. Hughson, P. E. Wright, R. L. Baldwin, *Science* **1990**, *249*, 1544–1548.
[34] H. Huttunen, J. C. Sherman, unpublished results.
[35] J. O. Freeman, D. Wallhorn, J. C. Sherman, unpublished results.
[36] a) I. Slavik, *Biochim. Biophys. Acta* **1982**, *694*, 1–25; b) G. V. Semisotnov, N. A. Rodionova, O. I. Razgulyaev, V. N. Uversky, A. F. Gripas, R. I. Gilmanshin, *Biopolymers* **1991**, *31*, 119–128.
[37] W. R. P. Scott, E. S. Seo, H. Huttunen, D. Wallhorn, J. C. Sherman, S. K. Straus, *Proteins Struct. Funct. Bioinf.* **2006**, *64*, 719–729.
[38] E. F. Pettersen, T. D. Goddard, C. C. Huang, G. S. Couch, D. M. Greenblatt, E. C. Meng, T. E. Ferrin, *J. Comput. Chem.* **2004**, *25*, 1605–1612.
[39] a) A. J. Wassner, J. A. Hurt, J. D. Lear, K. S. Akerfeldt, *Org. Lett.* **2002**, *4*, 1647–1649; b) C. F. W. Becker, M. Oblatt-Montal, G. G. Kochendoerfer, M. Montal, *J. Biol. Chem.* **2004**, *279*, 17483–17489.
[40] J. Hauert, J. Fernandez-Carneado, O. Michielin, S. Mathieu, D. Grell, M. Schapira, O. Spertini, M. Mutter, G. Tuchscherer, T. Kovacsovics, *ChemBioChem* **2004**, *5*, 856–864.
[41] N. E. Shepherd, H. N. Hoang, V. S. Desai, E. Letouze, P. R. Young, D. P. Fairlie, *J. Am. Chem. Soc.* **2006**, *128*, 13284–13289.
[42] a) Q.-H. Dai, C. Tommos, E. J. Fuentes, M. R. A. Blomberg, P. L. Dutton, A. J. Wand, *J. Am. Chem. Soc.* **2002**, *124*, 10952–10953; b) R. L. Koder, P. L. Dutton, *Dalton Trans.* **2006**, 3045–3051.
[43] a) W.-W. Li, P. Hellwig, M. Ritter, W. Haehnel, *Chem. Eur. J.* **2006**, *12*, 7236–7245; b) W. Haehnel, *Mol. Diversity* **2004**, *8*, 219–229.
[44] H. K. Rau, N. DeJonge, W. Haehnel, *Proc. Natl. Acad. Sci. USA* **1998**, *95*, 11526–11531.
[45] H. Rink, *Tetrahedron Lett.* **1987**, *28*, 3787–3790.
[46] M. M. Bradford, *Anal. Biochem.* **1976**, *72*, 248–254.
[47] L. Regan, A. Rockwell, Z. Wasserman, W. F. DeGrado, *Protein Sci.* **1994**, *3*, 2419–2427.
[48] T. M. Laue, B. D. Shah, T. M. Ridgeway, S. L. Pelletier, *Analytical Ultracentrifugation in Biochemistry and Polymer Science*, Royal Society of Chemistry, Cambridge, **1992**, pp. 90–125.
[49] M. L. Johnson, J. J. Correia, D. A. Yphantis, H. R. Halvorson, *Biophys. J.* **1981**, *36*, 575–588.
[50] J. Lebowitz, M. S. Lewis, P. Schuck, *Protein Sci.* **2002**, *11*, 2067–2079.
[51] J. Stetefeld, M. Jenny, T. Schulthess, R. Landwehr, J. Engel, R. A. Kammerer, *Nat. Struct. Biol.* **2000**, *7*, 772–776.
[52] P. K. Glasoe, F. A. Long, *J. Phys. Chem.* **1960**, *64*, 188–190.

Received: December 12, 2006
Published online: February 13, 2007

